THE JOURNAL OF PHYSICAL CHEMISTRY B

Article

pubs.acs.org/JPCB

Reorganization of Self-Assembled Dipeptide Porphyrin J-Aggregates in Water−Ethanol Mixtures

Raquel Teixeira,[†] Suzana M. Andrade,[†] Vanda Vaz Serra,[†,‡] Pedro M. R. Paulo,[†] Antonio Sánchez-Coronilla,[†] Maria G. P. M. S. Neves,[‡] José A. S. Cavaleiro,[‡] and Sílvia M. B. Costa*[,†]

[†]Centro de Química Estrutural, Complexo I, Instituto Superior Técnico, Universidade Técnica de Lisboa, Av. Rovisco Pais, 1049-001 Lisboa, Portugal

[‡]Departamento de Química, Universidade de Aveiro, Campus Universitário de Santiago, 3810-193 Aveiro, Portugal

Supporting Information

ABSTRACT: The self-assembly of a neutral *meso*-methoxyphenylporphyrin functionalized with a dipeptide glycilglycine substituent (MGG) in water and in water−ethanol mixtures was studied by absorption and fluorescence spectroscopy. In water, hydrophobic interactions and the noncovalent intermolecular hydrogen bonding between the terminal carboxylate group of one porphyrin and the hydrogen atoms of the pyrrolic nitrogens of another porphyrin originate nonspecific disorganized H- and J-aggregates. The addition of ethanol (0.1−25% v/v) to the water creates small clusters within which porphyrin J-aggregates reorganize as revealed by a narrow intense band detected by the Rayleigh light scattering (RLS) at 443 nm. Similar phenomenology is detected in SDS premicellar aggregates. Computational DFT calculations of a model dimer formation stabilized via intermolecular hydrogen bonding estimate an energy gain of −22 kJ mol^{-1} and a center-to-center and interplane distances between porphyrin moieties of 16.8 and 3.7 Å, respectively. The kinetics of the J-aggregate formation could be fitted with a time-dependent model, and an activation energy of 96 kJ mol^{-1} was estimated. The aggregate's morphology of MGG was followed by transmission electron microscopy (TEM) which showed rod-type structures of 5−8 μm evolving to spherical particles with increased ethanol content. Similar images and sizes were obtained in analogous samples using fluorescence lifetime imaging microscopy (FLIM) and dynamic light scattering (DLS). The formation of excitonically coupled supramolecular MGG structures of brickwork or staircase types is proposed in these water−ethanol mixtures.

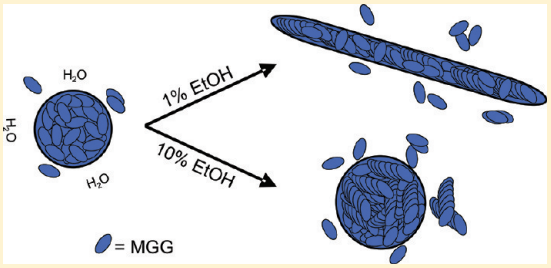

INTRODUCTION

Design of molecular assemblies based on self-association or aggregation for controlled size and shape is a simple and convenient method to construct supramolecular organizates with a wide range of possible applications: from models of heme proteins with relevance to catalysis, light-energy conversion, and nanostructured components of electronic and optoelectronic devices.[1−8]

Many porphyrins and metalloporphyrins form aggregates in solution; the nature and the extent of aggregation determine their response to photon excitation.[9] Depending on the geometry of the aggregation, these compounds can self-assemble to produce a variety of structures, ranging from stacked face-to-face arrangements called H-aggregates to side-to-side arrangements called J-aggregates as explained in Kasha excitonic theory.[10] The type of aggregation depends on the porphyrin structure, the nature of the metal ion, the solvent environment, and the temperature. A large body of investigation in this matter has been devoted to the water-soluble ionic *meso*-tetrakis(4-sulfonatophenyl)porphyrin (TSPP) due to the reported self-aggregation in acidic conditions.[11−16]

In recent years, a wide variety of nanometer-sized self-assembled porphyrins using noncovalent bonding have been reported.[17,18] In addition to spherical nanoparticles with diameters of 20−500 nm, the preparation of anisotropic bar-shaped assemblies of porphyrins, nanotubes, or nanorods were extensively reported.[19−24]

Functionalization of porphyrins with appropriate peripheral substituents can also result in the formation of porphyrin aggregates with different size and shapes displaying well-defined morphologies.[25−29]

It is well-known that hydrophobic porphyrins undergo aggregation processes in water-rich media.[30] The UV−vis spectra and AFM images of hydrophobic porphyrin−β-CD strongly suggest the formation of J-aggregates where the zinc porphyrin moieties are included within the β-cyclodextrin nanocavity of another ZnP-β-CD conjugate.[31]

Self-assembled nanostructures of a porphyrin−pentapeptide conjugate in water/THF mixtures were investigated as regards their morphology and chirality. The results obtained revealed the effect of the peptide secondary conformation and provide important insights toward the understanding of aggregation behavior of peptide containing porphyrins occurring in natural systems.[32]

Received: December 1, 2011
Revised: January 28, 2012
Published: January 31, 2012

In this study, we report the ability to reorganize the aggregate structures of *meso*-methoxyphenylporphyrin functionalized with a glycilglycine dipeptide substituent (MGG) (Figure 1).

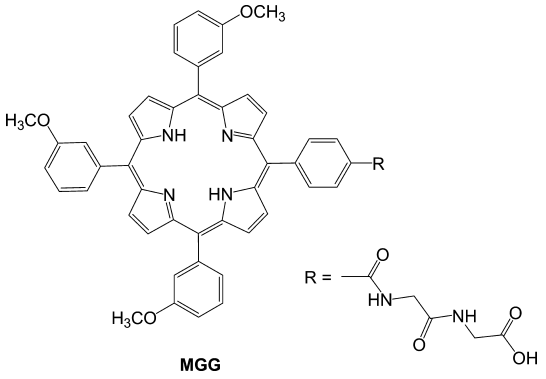

Figure 1. Molecular structure of the dipeptide glycilglycine porphyrin, MGG.

Controlled addition of small amounts of ethanol leads to the formation of organized J-type aggregates. In water and in water−ethanol mixtures, the sizes and shapes of these aggregates were characterized by transmission electron microscopy (TEM), dynamic light scattering (DLS), and fluorescence lifetime imaging microscopy (FLIM). The steady-state absorption and fluorescence and time-resolved fluorescence were also employed to describe the kinetics and photophysics of MGG self-assemblies.

EXPERIMENTAL SECTION

Materials. Synthesis of MGG was performed according to procedures commonly used for coupling amino acids to carboxylic porphyrins.[33] The activated ester of 5-(4-carboxyphenyl)-10,15,20-tris(3-methoxyphenyl)porphyrin (obtained after treatment with thionyl chloride, followed by addition of *N*-hydroxysuccinimide) was added to a mixture of glycil−glycine (Gly −Gly) with an excess of K_2CO_3 in DMSO and was left overnight under stirring at 40 °C. After work-up procedures, the porphyrin MGG was obtained in 93% yield. The structure of this porphyrin dipeptide derivative was confirmed by NMR, UV−vis spectroscopy, and mass spectrometry (FAB^+) (see Supporting Information).

Stock solutions of MGG porphyrin in DMSO (0.25 mM) were prepared, stored in the dark, and used within a month of preparation. Samples were prepared by dilution of a small aliquot (<1%) of DMSO stock solution and were left to stabilize overnight.

Sodium dodecyl sulfate (SDS), dodecyltrimethylammonium chloride (DTAC), and 1,2-dimirystoyl-*sn*-glycero-3-phosphocholine (DMPC, >99% purity) were purchased from Sigma-Aldrich and used as received. Citrate−phosphate buffer was employed for 2.5 < pH < 7.0 solutions, and the more acidic or more alkaline pH values were obtained by adding a few drops of highly concentrated solutions of HCl and NaOH, respectively. MGG solutions were prepared with spectroscopic grade organic solvents and/or bidistilled water.

Immobilized samples for FLIM measurements (see below) were prepared in cleaned and hydrophilized glass slides (5 min in H_2O_2/H_2SO_4 1:3) by spin-coating with an aliquot of each MGG solution.

Spectroscopic Data. The electronic extinction spectra were recorded in a Jasco V-560 UV−vis absorption spectrophotometer. Resonance light scattering (RLS) spectra were carried out in a Fluorolog Tau-3 spectrofluorimeter, by synchronous excitation and emission scanning in the right angle geometry, and corrected by subtracting the corresponding blank sample.[34−36] Fluorescence steady-state measurements were performed in the same instrument. Corrected spectra were obtained using the correction file provided with the instrument. All the spectra were recorded at room temperature using a 1 cm path length quartz cuvette.

Fluorescence Lifetime Measurements. Fluorescence lifetimes were also obtained with time-correlated single-photon counting (TC-SPC) technique using commercial equipment Microtime 200 from Picoquant GmbH. Excitation was achieved using a pulsed laser diode head at 405 nm, with varied repetition rate (10, 20, or 40 MHz). A band-pass filter with transmission in the range 600−800 nm was used to eliminate backscattered light in the photomultiplier tube from Picoquant (model PMA-182).[37] Data analysis was performed by a deconvolution method using a nonlinear least-squares fitting program, based on the Marquardt algorithm. The goodness of the fit was evaluated by the usual statistical criteria and by visual inspection of the weighted residuals distribution and the autocorrelation function.

Fluorescence Lifetime Imaging Microscopy (FLIM). FLIM was performed in the same setup, and a more detailed description may be found elsewhere.[38] Briefly, the 638 nm excitation light from a pulsed diode laser was focused by an oil immersion objective ×100 with 1.3 NA into the sample. Fluorescence was collected by the same microscope objective, passed through the dichroic mirror and appropriate band-pass filter (695AF55 Omega optical), and focused through a pinhole (50 μm), to reject out-of-focus light, onto a single-photon counting avalanche photodiode SPAD (Perkin-Elmer) whose signal was processed by TimeHarp 200 TC-SPC PC-board (PicoQuant) working in the special Time-Tagged Time-Resolved Mode, which stores all relevant information for every detected photon.

Transmission Electron Microscopy (TEM). TEM images were obtained with a Hitachi H-8100 electron microscope operated at 200 kV. A drop of MGG solution was deposited and air-dried in a carbon/Formvar-coated copper grid.

Dynamic Light Scattering (DLS). DLS measurements were performed in a Brookhaven Instruments (BI-200SM goniometer and BI-9000AT correlator) using a He−Ne laser (632.8 nm, 35 mW, model 127, Spectra Physics) and an avalanche photodetector. Measurements were carried out at 20 °C, at a scattering angle of 90°, with glass cylindrical cells submerged in decaline. Each sample measurement was repeated three times. Autocorrelation functions were analyzed using the analysis package CONTIN (Brookhaven).

Computational DFT Calculations. All structures were optimized in gas phase as real minima by using density functional theory (DFT)-based approaches, in the context of the Becke's three-parameter hybrid functional with gradient correction provided by the Lee−Yang−Parr functional (B3LYP)[39,40] with the cc-pVDZ basis set. The quantum mechanical computations have been carried out using the Gaussian 03 software.[41]

RESULTS AND DISCUSSION

Absorption and Emission Spectroscopy in Organic Solvents. The porphyrin MGG is hydrophobic and solubilizes

dx.doi.org/10.1021/jp2115719 | *J. Phys. Chem. B* 2012, 116, 2396−2404

well in dimethyl sulfoxide (DMSO). The absorption spectrum of MGG in DMSO is typical for a common free base porphyrin and exhibits a Soret band at 419 nm and four Q bands at 641, 588, 546, and 513 nm corresponding to $Q_x(0,0)$, $Q_x(1,0)$, $Q_y(0,0)$, and $Q_y(1,0)$, respectively. The fluorescence emission spectrum presents two vibronic bands centered at 650 and 718 nm which are independent of the excitation wavelength. Collection of light at these wavelengths produces an excitation spectrum which nearly coincides with the absorption spectrum.

Aqueous Solutions: pH Effect. In water at pH = 7.3 a sharp red-shifted band (λ = 443 nm) is observed (Figure 2A).

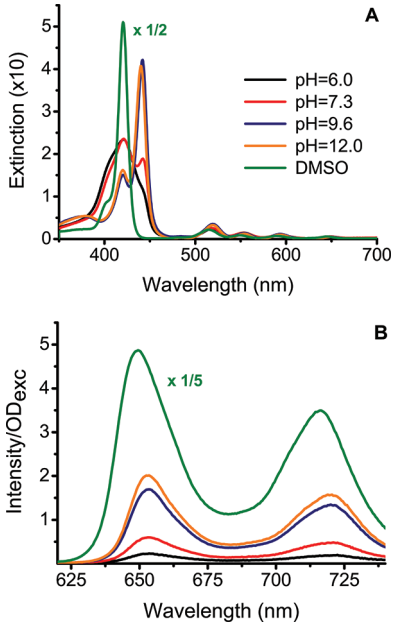

Figure 2. (A) UV–vis and (B) emission spectra of MGG (2 μM) in aqueous solutions (pH 6–12) and in DMSO. Excitation was performed in the J-aggregate band (440 nm) for the aqueous solutions and at 400 nm for MGG in DMSO.

This band is always accompanied by a shoulder at a wavelength characteristic of the monomer absorption (λ = 418 nm) and a broad band (λ = 367 nm). The sharp narrow band is likely to correspond to a J-aggregate, whereas the blue-shifted broad band is probably due to the presence of an H-aggregate as deduced from excitonic theory.[10] In this molecule, the co-existence of J- and H-aggregates is probably due to coupled porphyrins which may have transition dipoles whose axis form oblique angles.

The aggregate bands are strongly affected by the pH of the aqueous solution. The sharp absorption centered at 443 nm is always present in a wide pH range from 6 to 12, but it is predominant at pH > 7.3.

The fluorescence spectra obtained are basically independent of the excitation wavelength (400 or 440 nm) showing the expected two emission bands from the monomer at higher pHs (>2.9, Figure 2B) and a structureless intense band (λ_{em} = 685 nm, data not shown) due to the monomeric dicationic species at pHs $\leq$ 2.9. The excitation spectra obtained by collecting the emission at 650 nm (Figure 3A) show that the emission has contributions from both the monomer and from the J-aggregate species. The RLS effect is observed as increased scattering intensity at or very near the wavelength of absorption of an aggregated molecular species. The RLS spectra run at different pHs (Figure 3B) confirm the existence of a pronounced peak due to the aggregate formation.

Water–Ethanol Mixtures. Hydrophobic effect leads to an immediate self-association of MGG in water and to the formation of MGG disordered aggregates. The mixture with water-structure breakers, such as ethanol, can lower this effect promoting the rearrangement of the aggregates. It is known that minute amounts of ethanol are capable of disrupting the hydrogen-bonding network between water molecules (hydrophobic hydration layer), weakening the hydrophobic effect.

Addition of ethanol to nonspecific disorganized aqueous aggregates of MGG in water results in an apparent reorganization of porphyrin molecules as seen by the sharp red-shifted absorption band (λ = 443 nm, fwhm ~ 530 cm^{-1} vs fwhm ~ 730 cm^{-1} of the monomer in pure ethanol), which is likely indicative of an intrinsic tendency toward the arrangement into J-aggregate structure.

Fluorescence emission spectra, with excitation either at 420 nm (ethanol monomer) or at 440 nm (aggregate in water–ethanol mixtures), show that the observed formation and increase of J-aggregate absorption band is accompanied by an increase in fluorescence intensity (Figure 4A,B). In fact, the maximum emission obtained at 650 and 720 nm with excitation at 420 nm corresponds approximately to one-third of the emission detected from the porphyrin monomer in pure ethanol (data not shown).

The excitation spectra of all porphyrin aggregates correlate with the corresponding absorption spectra (Figure 4C). A further unequivocal confirmation to the assignment of a MGG J-aggregate was obtained from the RLS spectra. The narrow band at 446 nm peak grows with the increase of ethanol content in the mixture (Figure 4D).

Similar studies with Zn metalated and esterified porphyrins did not show the formation of the specific J-aggregates (Figure 5A,B). In these compounds it is not possible to establish a noncovalent intermolecular hydrogen bonding between the terminal carboxylic

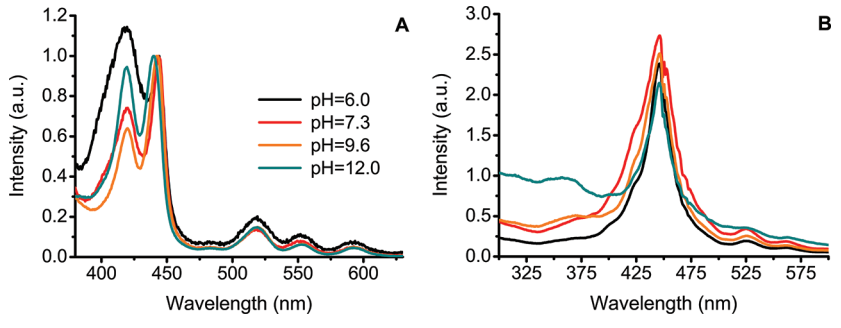

Figure 3. (A) Excitation (λ_{em} = 650 nm) and (B) RLS spectra of MGG (2 μM) in aqueous solutions (pH 6–12).

dx.doi.org/10.1021/jp2115719 | J. Phys. Chem. B 2012, 116, 2396–2404

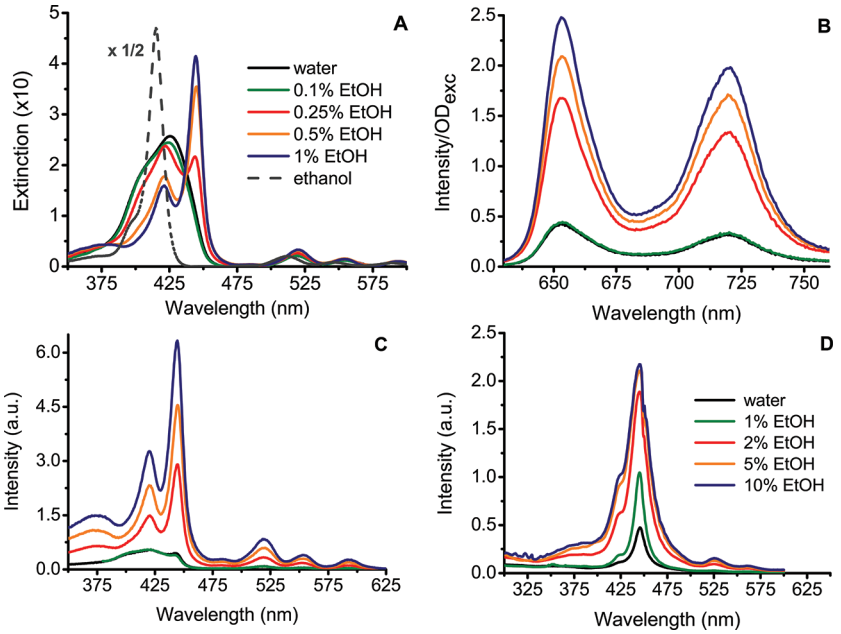

Figure 4. UV–vis (A), emission (B), and excitation (C) spectra of MGG (2 μM) in water–ethanol binary mixtures (0–1% of EtOH); λ_{exc} = 440 nm in (B) and λ_{em} = 650 nm in (C). (D) RLS spectra for an extended range of water/ethanol binary mixtures (0–10% of EtOH).

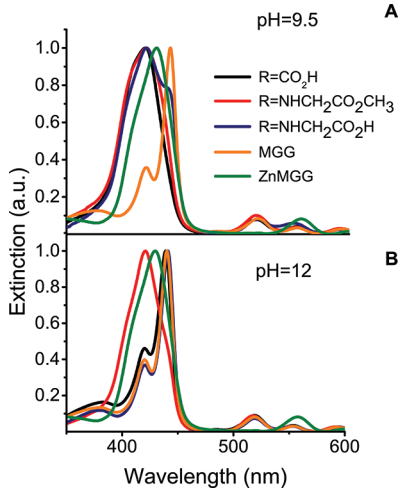

Figure 5. Extinction spectra of different R-substituted porphyrins related to MGG in basic media: (A) pH 9.5 and (B) pH 12.

group and the hydrogen atoms of pyrrolic nitrogens. This supports the assumption made for the driving force of MGG J-aggregation. Furthermore, since the monosubstituted glycine exhibits the J-aggregate only at pH = 12, it seems that a minimum arm length is required to connect the porphyrin macrocycle to the terminal carboxylic group, in order to be able to generate the structural rearrangement of the aggregate (Figure 5B).

Fluorescence Lifetimes. Fluorescence lifetimes of both monomer and J-aggregates in water–ethanol mixtures were determined. In pure ethanol, MGG is nearly monomeric with a long lifetime of about 10 ns. By contrast, a triexponential decay is obtained in water with a main component of 0.3 ns, an intermediate component lifetime of 1.4 ns, and a contribution of a longer lifetime of 9.9 ns corresponding to the monomer. The addition of small amounts of ethanol to water resulted in a decrease in the fractional amplitude of the shortest lifetime component with the simultaneous increase of the intermediate one (see Table 1). The average lifetime is sensitive to the ethanol percentage showing a clear transition point at about

Table 1. Fluorescence Lifetimes of MGG in Water–Ethanol Binary Mixtures; λ_{exc} = 405 nm and λ_{em}= 600–800 nm

	disordered aggregates		ordered aggregates		monomer		
% (v/v) EtOH	A_1 (%)	τ_1 (ns)	A_2 (%)	τ_2 (ns)	A_3 (%)	τ_3 (ns)	χ^2
0	**40**	**0.3**	27	1.4	33	9.9	1.109
1	19	0.5	**61**	**1.8**	20	4.4	1.074
5	18	0.6	**71**	**2.0**	12	6.9	1.109
10	18	0.6	**69**	**2.0**	13	5.7	1.010
25	10	0.7	**59**	**2.3**	31	4.8	1.081
27.5	10	0.8	**61**	**2.5**	28	5.9	0.993
30	14	0.9	**58**	**2.7**	29	8.8	1.035
32.5	8	1.0	28	2.8	**65**	**11.3**	1.056
35	4	0.9	10	2.5	**87**	**11.6**	1.038
40	1	1.2			**99**	**11.7**	1.104
100	1	0.6			**99**	**10.0**	1.150

30% EtOH. Above this point, the average lifetime increases and reaches the value of the monomer fluorescence lifetime. It is well-known that above a critical ethanol mole fraction corresponding to 27.5% v/v EtOH the microaggregation of ethanol occurs. Local heterogeneity and hydrophobicity effects are observed upon the introduction of small amounts of ethanol in water, causing a breakdown of the water structure. In fact, the nonideality of water–ethanol mixtures is linked with the formation of ethanol clusters which are maintained by cooperative interactions of hydrophobic and hydrophilic nature among participating molecules.[42–44]

Ionic Surfactants. Parallel studies of this porphyrin in sodium dodecyl sulfate (SDS) leads also to formation of identical J-type aggregates. The extinction spectra and RLS spectra (Figure 6A) show the same J-aggregate in the negative SDS premicellar clusters which by analogy with the water–

dx.doi.org/10.1021/jp2115719 | J. Phys. Chem. B 2012, 116, 2396–2404

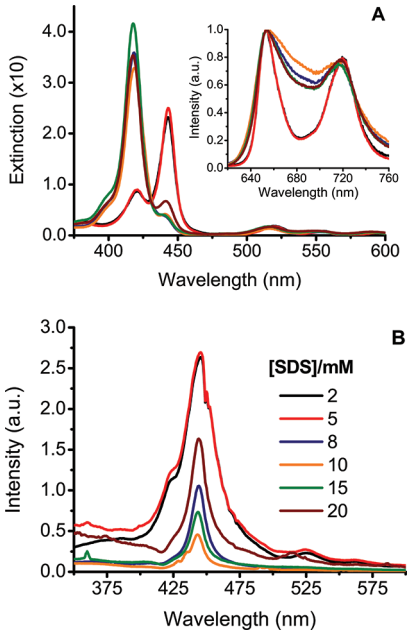

Figure 6. UV/vis (A) and RLS (B) spectra of MGG (2 μM) in sodium dodecyl sulfate (SDS) aqueous solutions (2, 5, 8, 10, 15, and 20 mM). Inset of (A) emission spectra, λ_{exc} = 440 nm.

ethanol clusters may serve as templates for the formation of an ordered J-aggregate. Fluorescence lifetimes in the premicellar aggregates ([SDS] = 5 mM) are slightly higher than those in water−ethanol mixtures, perhaps reflecting a more hydrophobic environment (data not shown). Above the critical micelle concentration (cmc, 8 mM), in SDS micelles, the MGG monomer prevails, but around 10% of the J-aggregate remains. The extinction spectra shows that at higher surfactant concentration the J-aggregate starts growing again perhaps due to alterations in the micellar structure (Figure 6B). The excitation on the aggregate indicates that the emission has a major contribution from the neutral porphyrin, but the dicationic porphyrin emission increases in the SDS micelle (inset of Figure 6A).

By contrast, with the positive surfactant dimethyltrimethylammonium chloride (DTAC), a composition of the broad band and the narrow is observed in the whole surfactant concentration below and above the cmc. Also, in 1,2-dimiristoyl-*sn*-glycero-3-phosphocholine (DMPC) vesicles a complex mixture of monomer and aggregates remains well above the critical aggregation concentration.

Kinetics of Porphyrin (MGG) J-Aggregates. The initial nonspecific MGG aggregates in water are amorphous and can be reorganized into ordered aggregates in the water−ethanol clusters which are formed at molar fractions of ethanol above 27.5% v/v. It is assumed that large aggregate sizes are formed upon the interaction between small solvent preclusters in the solution and the monomers. Therefore, the aggregate concentration measured by the extinction peak grows exponentially with the molar fraction of ethanol.

Since the aggregation process occurs in the ground state, it was possible to follow the kinetics at different temperatures monitoring either the growth in extinction at 442 nm or the decrease in extinction at 418 nm (Figure 7). Porphyrin reorganization kinetics of MGG in water−ethanol mixtures with 25% (v/v) of alcohol were studied. In Figure 8, the growth of the spectroscopic aggregate (λ_{abs} = 443 nm) is monitored as

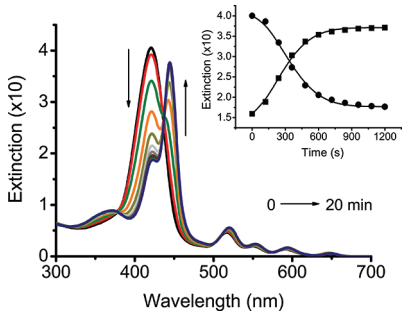

Figure 7. Extinction spectra of MGG (1 μM) in water−ethanol 25% at 35 °C as a function of time. Inset: kinetic curves obtained from extinction at 418 nm (circles) and 442 nm (squares).

a function of time at different temperatures. Reorganization of MGG is a temperature-dependent phenomenon that occurs faster at high temperatures but maintaining the same sigmoidal growth profile at every temperature.

The kinetic behavior was fitted to a model equation which has been used for autocatalytic J-aggregate formation

$$\frac{\mathrm{Ext} - \mathrm{Ext}_\infty}{\mathrm{Ext}_0 - \mathrm{Ext}_\infty} = (1 + (m-1)\{k_0 t + (n+1)^{-1}(k_c t)^{n+1}\})^{-1/(m-1)} \quad (1)$$

where k_0 is the rate constant for the uncatalyzed growth, k_c is the rate constant for the catalyzed pathway, n describes the growth of the chromophore assembly as a power function of time, and m is related to the size of the critical nucleous, the formation of which is the rate-determining step in the process.[45−47] The kinetic parameters obtained are shown in Table 2.

A good linear fit of this equation to the progression of the extinction aggregation band was obtained as shown in both Figures 7 and 8. From the Arrhenius plot of the rate constant, the activation energy of E_a = 96 kJ mol^{-1} was estimated.

The growth of the spectroscopic aggregate was also studied for different concentrations of MGG. No fitting was obtained, which means that this rearrangement is not concentration-dependent and the process is not diffusion-controlled.

The coherence length (N_c) of the spectroscopic aggregate was calculated taking into account thermal line broadening effects, using eq 2.[48]

$$(N_c + 1)^2 \cos\left(\frac{\pi}{N_c + 1}\right) = \frac{3\pi^3}{(4\pi\lambda kT)^{1/2}}\Delta E \quad (2)$$

This calculation indicates that the number of porphyrin units involved in the spectroscopic aggregate should be ~15, which corresponds to an aggregate length of about 5−7 nm.

The porphyrin rearrangement starts with ethanol fractions as low as 0.1% (v/v) in water−ethanol binary mixtures. So, disordered aggregates are "frozen" within the surrounding water network until a perturbation in the water ordered structure increases the rotation/diffusion freedom of the porphyrins. This drives the structural rearrangement of the aggregates that occurs with an energetic gain due to the noncovalent intermolecular hydrogen bonds between the carboxylate of one porphyrin with hydrogen atoms of pyrrolic nitrogens of the next porphyrin within the aggregate.

Some parallel can be found with the phenomenology of structural modifications of albumin BSA.[49] In this study it is concluded that amorphous aggregates can reorganize into

dx.doi.org/10.1021/jp2115719 | J. Phys. Chem. B 2012, 116, 2396−2404

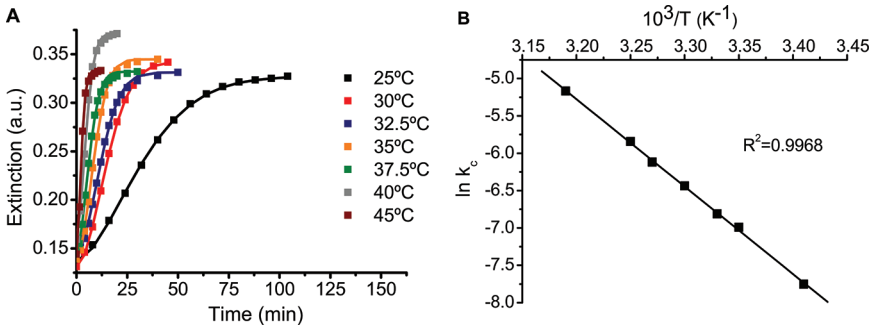

Figure 8. Kinetic profiles (A) obtained for MGG aggregation at different temperatures from 25 to 45 °C. A linear Arrhenius plot (B) is observed, giving an activation energy (E_a) of 96 kJ mol^{-1}.

Table 2. Kinetic Data for the Reorganization of MGG Aggregates, at Different Temperatures

T (°C)	k_0 (×10^{-3} s^{-1})	k_c (×10^{-3} s^{-1})	m	n
20	0.2	0.6	1.5	1.7
25	0.2	1.4	1.5	1.7
27.5	0.2	1.8	1.5	1.7
30	0.3	2.5	1.6	1.7
32.5	0.4	3.6	1.8	1.8
35	0.8	4.6	1.8	1.9
40	2	9.5	2.2	2.6

protofibrils in the low concentration regime and at basic pH = 8.9, due to the resulting balance of nonspecific interactions (electrostatic, hydrophobic, and H-bond). The overall reorganization is a thermally activated process with an energetic barrier of 121 kJ mol^{-1} (for a 2−4 nm length structure) which is similar to the activation energy involved in the reorganization of our MGG porphyrin J-aggregate.

Morphology and Sizes of MGG Aggregates. The samples of MGG in water−ethanol mixtures were separately examined using dynamic light scattering (DLS), transmission electron microscopy (TEM), and fluorescence lifetime imaging microscopy (FLIM).

a. Dynamic Ligth Scattering (DLS). The DLS measurements represented by the autocorrelation curves (Figure 9)

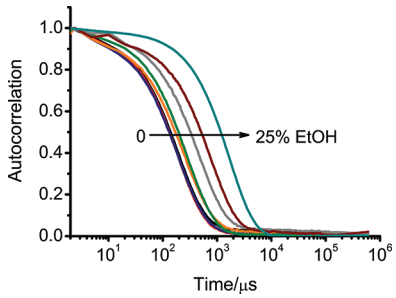

Figure 9. Autocorrelation data obtained in DLS experiments for MGG (2 μM) in water/ethanol binary mixtures with 0, 0.1, 0.25, 0.5, 1, 5, 10 and 25% (v/v) of EtOH.

show the dependence of the percentage of ethanol in the MGG samples. Assuming a spherical model for the aggregates, an average hydrodynamic diameter of 80 nm was obtained in pure water, but the addition of ethanol increased the average aggregate size which reached the diameter of 540 nm when the ethanol concentration was 25% v/v in the mixture (Table 3).

Table 3. Hydrodynamic Radii of MGG Obtained from DLS Experiments

% EtOH (v/v)	av radius (nm)	% EtOH (v/v)	av radius (nm)
0	40 ± 3.8	1	56 ± 6.5
0.1	39 ± 4.2	5	79 ± 9.4
0.25	42 ± 5.1	10	124 ± 10.8
0.5	55 ± 5.2	25	270 ± 18.9

Curiously, some autocorrelation curves obtained for 1% v/v ethanol gave evidence for the existence of large particles (diameter ∼ 2000 nm) which also depended on the angle of observation (60°, 90°, and 120°).

b. Transmission Electron Microscopy (TEM). The aggregates' morphology was examined by transmission electron microscopy (TEM). As depicted in Figure 10, well-defined, completely regular and isolated nanospheres with an average diameter of ca. 80 nm were formed from the self-assembly of MGG, 5 μM, in water. However, the increase in MGG concentration to 50 μM changed the aggregate morphology to 5−8 μm rodlike structures. The addition of 1% v/v ethanol keeps the aggregate's shape and size, but further addition up to 10% v/v ethanol changes the rods into spheres of ϕ = 80−100 nm which, at 25% v/v ethanol, reach the diameter ϕ = 550−690 nm (Figure 11). Under these conditions, it can be seen from the TEM images that the spherical particles are completely dispersed and do not tend to associate with each other at any of the water−ethanol ratio tested. In addition, the sizes obtained for the spherical particles are in good agreement with DLS results. The large diameters obtained at 1% v/v ethanol were an indication that some rodlike structures already coexisted with spherical ones at lower MGG concentrations as those used in DLS measurements. These structures are clearly absent at higher ethanol volumes regardless the porphyrin concentration used. Even though a direct comparison cannot be established between the particles association in suspension and those dried and deposited on a substrate, it is worth to note the similarity between the electronic absorption spectra of MGG in solution and of that deposited in the presence of ethanol (15−25% v/v, see Figure S1, Supporting Information), whereas in the absence of the organic solvent distinct spectra are obtained.

c. Fluorescence Lifetime Imaging Microscopy (FLIM). Very similar images of MGG samples deposited on a glass coverslip can be viewed by FLIM in water and in water−ethanol mixtures, as shown in Figure 12. This technique gives an additional support to the elucidation of shapes, but the optical resolution is diffraction-limited, $\sim\lambda_{exc}/2$. Thus, the fluorescence lifetime images of the aggregates are collected at ∼300 nm spatial

dx.doi.org/10.1021/jp2115719 | J. Phys. Chem. B 2012, 116, 2396−2404

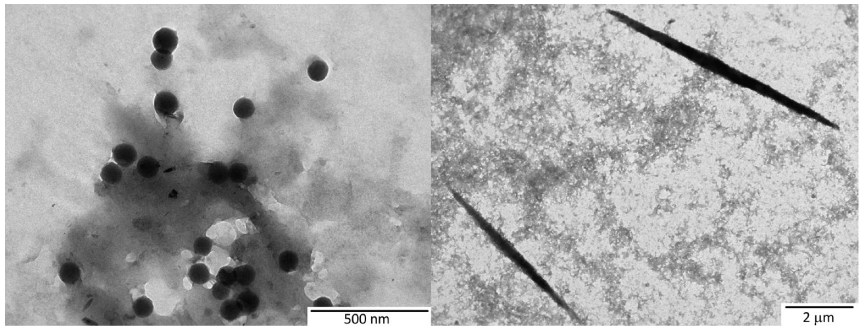

Figure 10. TEM images of MGG aggregates drop-cast from an aqueous solution of [MGG] = 5 μM (left) and of [MGG] = 50 μM (right).

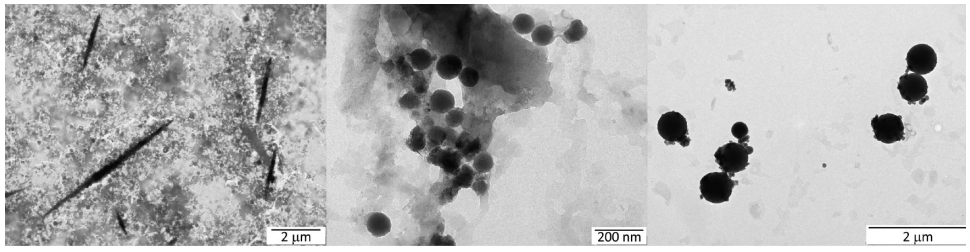

Figure 11. TEM images of MGG aggregates in aqueous mixture with different amounts of ethanol: 1%; 10%, and 25% v/v (from left to right). [MGG] = 50 μM.

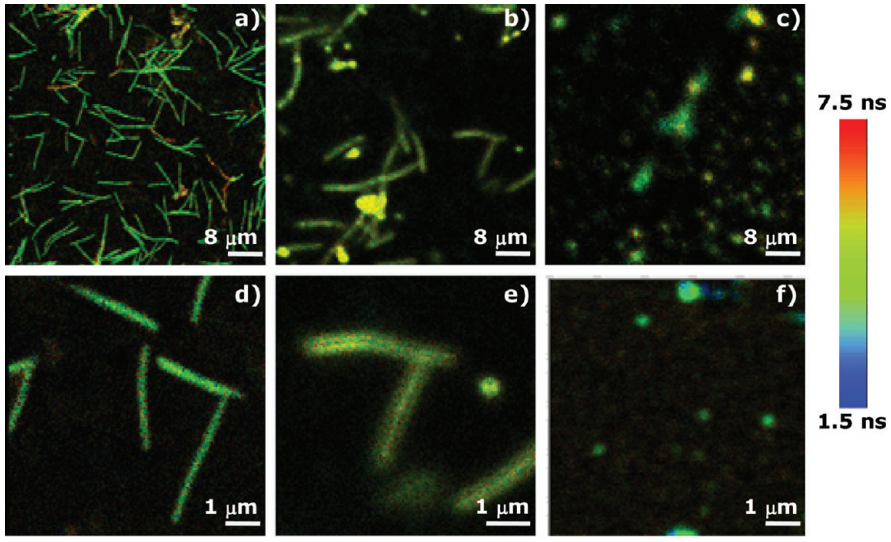

Figure 12. FLIM images of MGG aggregates obtained from drop-cast of an aqueous mixture with different amounts of ethanol: (a, d) 0%, (b, e) 1%, and (c, f) 25% v/v. Bottom images are zooms of certain regions of those on top. [MGG] = 50 μM.

resolution and (sub)nanosecond temporal resolution. Lifetimes obtained using an exponential model agree well with those obtained in solution. The prevalence of an intermediate lifetime ($\tau \sim 1.5-2.5$ ns) for these deposited samples, let us assign it to the J-aggregates. Furthermore, in plain water, rodlike structures are obtained which coexist with spherical ones upon a small addition of ethanol (1% v/v). The spherical shape predominates for the aggregates induced at 25% v/v ethanol with sizes consistent with those obtained by TEM (and in solution using DLS).

Theoretical Calculations. The driving force for the aggregate formation is likely to be the intermolecular hydrogen bonding between the oxygen atom of the terminal carboxyl group of one porphyrin molecule and the hydrogen atoms of the pyrrolic nitrogens of another porphyrin. This interaction model between MGG porphyrin units assembled in the J-aggregate was assessed by computational DFT calculations in order to suggest a suitable molecular geometry.

For computational reasons we have performed the calculations with the dimeric structure depicted in Figure S2 of the Supporting Information as a model of the hydrogen bond interactions. In this structure the carboxylate group of one porphyrin derivative interacts with the hydrogen atom of the pyrrolic nitrogen of the second porphyrin ring and vice versa (O−H distances around 1.6 Å). The energy gain of −22 kJ/mol is in the range of hydrogen-bonding energy and resembles that obtained elsewhere[50] for porphyrin intermolecular hydrogen-bonding J-aggregates. The center-to-center and interplane distances between porphyrin moieties are ca. 16.8 and 3.7 Å, respectively. Noteworthy is the good agreement for the interplane

dx.doi.org/10.1021/jp2115719 | J. Phys. Chem. B 2012, 116, 2396−2404

distance with that of 3.6 Å obtained from crystallographic determinations for adjacent planes of porphyrin J-aggregates.[51] The interplane distance and the dihedral angle (ca. 5°) between the nitrogen atoms of both porphyrin moieties suggest the formation of excitonically coupled J-aggregates, in agreement with the narrow J-aggregate band in the extinction spectra.

On the basis of the theoretical results, we tentatively propose the staircase-type and brickwork-type arrangements shown in Figure 13 as representative of the supramolecular porphyrin

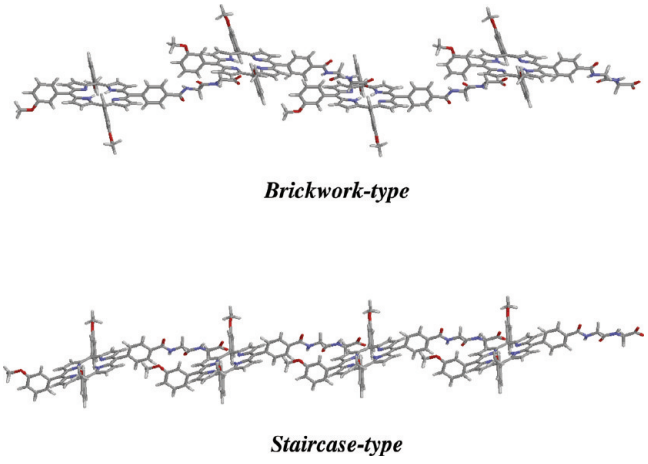

Figure 13. Schematic model for the J-aggregates showing brickwork- and staircase-type proposed structures.

aggregates. Spectroscopic aggregates should not have more than a few tens of MGG coupled units. Thus, none of the macroscopic structures detected by TEM or DLS can be attributed to single spectroscopic aggregates but rather to a mixture of spectroscopic aggregates.

CONCLUSIONS

The self-assembly of a neutral *meso*-methoxyphenylporphyrin functionalized with a glycilglycine substituent (MGG) in water and in water−ethanol mixtures was studied by absorption and fluorescence spectroscopy.

In water, hydrophobic interactions and the noncovalent intermolecular hydrogen bonding between the terminal carboxylate group of one porphyrin and the hydrogen atoms of pyrrolic nitrogens of another porphyrin originate nonspecific H- and J-aggregates. The initial solubilization of porphyrin in water originates a disordered kinetically controlled aggregate.

The addition of small amounts of ethanol forms "clusters" which break the water network and lead to the structural rearrangement of the porphyrin aggregates.

The spectroscopic, kinetic, and imaging data obtained in the present work point to the enhancement and reorganization of excitonically coupled self-assembly of MGG porphyrin monomeric entities into larger supramolecular structures in water−ethanol mixtures.

ASSOCIATED CONTENT

Supporting Information

Structural characterization of porphyrin MGG, Figures S1 and S2, and technical details of the theoretical calculations. This material is available free of charge via the Internet at http://pubs.acs.org.

AUTHOR INFORMATION

Corresponding Author

*E-mail: sbcosta@ist.utl.pt.

Notes

The authors declare no competing financial interest.

ACKNOWLEDGMENTS

Thanks are due to Fundação para a Ciência e a Tecnologia (FCT, Portugal) for 3° Quadro Comunitário de Apoio (FEDER); FCT/Re-equipment Project 115/QUI/2005 and PTDC/QUI/64112/2006. R. Teixeira, V. V. Serra, and A. S. Coronilla, grants SFRH/BD/28122/2006 SFRH/BD/39006/2007 and SFRH/BPD/64898/2009. S. M. Andrade and P. M. R. Paulo, Program Ciência 2007, 2008. Thanks are also due to Prof. J. M. G. Martinho for the use of the DLS equipment, to Ms. R. F. Correia for helping with DLS experiments, and to the CICA - Centro Informático Científico de Andalucia (Spain) for computational time.

REFERENCES

(1) Whitesides, G. M.; Grzybowski, B. A. *Science* **2002**, *295*, 2418−2421.
(2) Lehn, J.-M. *Angew. Chem., Int. Ed.* **1990**, *29*, 1304−1319.
(3) Winters, M. U.; Dahlstedt, E.; Blades, H. E.; Wilson, C. J.; Frampton, M. J.; Anderson, H. L.; Albinsson, B. *J. Am. Chem. Soc.* **2007**, *129*, 4291−4297.
(4) Hasobe, T.; Saito, K.; Kamat, P. V.; Troiani, V.; Hongjin Qiu, H.; Solladié, N.; Kim, K. S.; Park, J. K.; Kim, D.; D'Souza, F.; Fukuzumi, S. *J. Mater. Chem.* **2007**, *17*, 4160−4170.
(5) Belanger, S. S.; Hupp, J. T. *Angew. Chem., Int. Ed.* **1999**, *38*, 2222−2224.
(6) Paulo, P. M. R.; Gronheid, R.; De Schryver, F. C.; Costa, S. M. B. *Macromolecules* **2003**, *36*, 9135−914.
(7) Romeo, A.; Castriciano, M. A.; Scolaro, L. M. S. *J. Porphyrins Phthalocyanines* **2010**, *14*, 713−721.
(8) Schwab, A. D.; Smith, D. E.; Bond-Watts, B.; Johnston, D. E.; Hone, J.; Johnson, A. T.; de Paula, J. C.; Smith, W. F. *Nano Lett.* **2004**, *4* (7), 1261−1265.
(9) De Luca, G.; Romeo, A.; Scolaro, L. M.; Pasternack, R. F. *Chem. Commun.* **2010**, *46*, 389−391.
(10) Kasha, M.; Rawls, H. R.; El-Bayoumi, M. *Pure Appl. Chem.* **1965**, *11* (34), 371−392.
(11) Ohno, O.; Kaizu, Y.; Kobayashi, H. *J. Chem. Phys.* **1993**, *99*, 4128−4139.
(12) Akins, D. L.; Zhu, H.-R.; Guo, C. *J. Phys. Chem.* **1994**, *98*, 3612−3618.
(13) Maiti, N. C.; Mazumdar, S.; Periasamy, N. *J. Phys. Chem. B* **1998**, *102*, 1528−1538.
(14) Andrade, S. M.; Costa, S. M. B. *Biophys. J.* **2002**, *82*, 1607−1619.
(15) Andrade, S. M.; Costa, S. M. B. *Chem.—Eur. J.* **2006**, *12*, 1046−1057.
(16) Friesen, B. A.; Nishida, K. R. A.; McHale, J. L.; Mazur, U. *J. Phys. Chem. C* **2009**, *113*, 1709−1718.
(17) Tachikawa, T.; Chung, H.-R.; Masuhara, A.; Kasai, H.; Oikawa, H.; Nakanishi, H.; Fujitsuka, M.; Majima, T. *J. Am. Chem. Soc.* **2006**, *128*, 15944−15945 and references therein..
(18) Tashiro, K.; Aida, T. *Chem. Soc. Rev.* **2007**, *36*, 189−197 and references therein..
(19) Harada, R.; Matsuda, Y.; Okawa, H.; Kojima, T. *Angew. Chem., Int. Ed.* **2004**, *43*, 1825−1828.
(20) Wang, Z.; Medforth, C. J.; Shelnutt, J. A. *J. Am. Chem. Soc.* **2004**, *126*, 15954−15955.
(21) Kojima, T.; Harada, R.; Nakanishi, T.; Kaneko, K.; Fukuzumi, S. *Chem. Mater.* **2007**, *19*, 51−58.
(22) Zhou, Q.; Li, C. M.; Li, J.; Cui, X.; Gervasio, D. *J. Phys. Chem. C* **2007**, *111*, 11216−11222.

(23) Kishida, T.; Fujita, N.; Sada, K.; Shinkai, S. *J. Am. Chem. Soc.* **2005**, *127*, 7298−7299.
(24) Hasobe, T.; Sandanayaka, A. S. D.; Wadac, T.; Arakic, Y. *Chem. Commun.* **2008**, 3372−3374.
(25) Choi, M. Y.; Pollard, J. A.; Webb, M. A.; McHale, J. L. *J. Am. Chem. Soc.* **2003**, *125*, 810−820.
(26) Doan, S. C.; Shanmugham, S.; Aston, E. D.; McHale, J. L. *J. Am. Chem. Soc.* **2005**, *127*, 5885−5892.
(27) Hosomizu, K.; Oodoi, M.; Umeyama, T.; Matano, Y.; Yoshida, K.; Isoda, S.; Niemi, M.; Tkachenko, N. V.; Lemmetyinen, H.; Hiroshi, H. *J. Phys. Chem. B* **2008**, *112*, 16517−16524.
(28) Serra, V. V.; Andrade, S. M.; Neves, M. G. P. M. S.; Cavaleiro, J. A. S.; Costa, S. M. B. *New J. Chem.* **2010**, *34*, 2757−2765.
(29) Sandanayaka, A. S. D.; Araki, Y.; Wada, T.; Hasobe, T. *J. Phys. Chem. C* **2008**, *112*, 19209−19216.
(30) Udal'tsov, A. V.; Kazarin, L. A.; Sinani, V. A.; Sweshnikov, A. A. *J. Photochem. Photobiol., A* **2002**, *151*, 105−119.
(31) Kiba, T.; Suzuki, H.; Hosokawa, K.; Kobayashi, H.; Baba, S.; Kakuchi, T.; Sato, S.-i. *J. Phys. Chem. B* **2009**, *113*, 11560−11563.
(32) Wang, Q.; Chen, Y.; Ma, P.; Lu, J.; Zhang, X.; Jiang, J. *J. Mater. Chem.* **2011**, *21*, 8057−8065.
(33) Serra, V. V.; Zamarrón, A.; Faustino, M. A. F.; Iglesias-de la Cruz, M. C.; Blázquez, A.; Rodrigues, J. M. M.; Neves, M. G. P. M. S.; Cavaleiro, J. A. S.; Juarranz, A.; Sanz-Rodríguez, F. *Bioorg. Med. Chem.* **2010**, *18*, 6170−6178.
(34) Parkash, J.; Robblee, J. H.; Agnew, J.; Gibbs, E.; Collings, P.; Pasternack, R. F.; de Paula, J. C. *Biophys. J.* **1998**, *74*, 2089−2099.
(35) Collings, P. J.; Gibbs, E. J.; Starr, T. E.; Vafek, O.; Yee, C.; Pomerance, L. A.; Pasternack, R. F. *J. Phys. Chem. B* **1999**, *103*, 8474−8481.
(36) Pasternack, R. F.; Bustamante, C.; Collings, P. J.; Giannetto, A.; Gibbs, E. J. *J. Am. Chem. Soc.* **1993**, *115*, 5393−5399.
(37) Paulo, P. M. R.; Costa, S. M. B. *J. Phys. Chem. C* **2010**, *114* (44), 19035−19043.
(38) Togashi, D. M.; Costa, S. M. B.; Sobral, A. J. F. N. *Biophys. Chem.* **2006**, *119*, 121−126.
(39) Becke, A. D. *J. Chem. Phys.* **1993**, *98*, 5648−5652.
(40) Lee, C.; Yang, W.; Parr, R. G. *Phys. Rev. B: Condens. Matter Mater. Phys.* **1988**, *37*, 785−789.
(41) Frisch, M. J.; et al. *Gaussian 03*; Gaussian, Inc.: Wallingford, CT, 2003.
(42) Matsumoto, M.; Nishi, N.; Furusawa, T.; Saita, M.; Takamuku, T.; Yamagami, M.; Yamaguchi, T. M. *Bull. Chem. Soc. Jpn.* **1995**, *68*, 1775−1783.
(43) Petong, P.; Pottel, R.; Kaatze, U. *J. Phys. Chem. A* **2000**, *104*, 7420−7428.
(44) Ferreira, J. A. B.; Costa, S. M. B. *Phys. Chem. Chem. Phys.* **2003**, *5*, 1064−1070.
(45) Pasternack, R. F.; Fleming, C.; Herring, S.; Collings, P. J.; de Paula, J.; DeCastro, G.; Gibbs, E. J. *Biophys. J.* **2000**, *79*, 550−560.
(46) Monti, D.; Massimo De Rossi, M.; Sorrenti, A.; Laguzzi, G.; Gatto, E.; Stefanelli, M.; Venanzi, M.; Luvidi, L.; Mancini, G.; Paolesse, R. *Chem.—Eur. J.* **2010**, *16*, 860−870.
(47) Görner, H.; Slavnova, T. D.; Chibisov, A. K. *J. Phys. Chem. B* **2010**, *114*, 9330−9337.
(48) Koti, A. S. R.; Taneja, J.; Periasamy, N. *Chem. Phys. Lett.* **2003**, *375*, 171−176.
(49) Vetri, V.; D'Amico, M.; Foderà, V.; Leone, M.; Ponzoni, A.; Sberveglieri, G.; Militello, V. *Arch. Biochem. Biophys.* **2011**, *508*, 13−24.
(50) Peng, X.; Huang, Y.; Gao, C.; Peng, J.; Komatsu, N.; Osuka, A.; Cao, Y. *J. Phys. Chem. C* **2010**, *114*, 18449−18454.
(51) Kano, K.; Fukuda, K.; Wakami, H.; Nishiyabu, R.; Pasternack, R. F. *J. Am. Chem. Soc.* **2000**, *122*, 7494−7502.